J. Phys. Chem. Solids Vol. 48, No. 1, pp. 79–89, 1987
Printed in Great Britain.

0022-3697/87 $3.00 + 0.00
Pergamon Journals Ltd.

EFFECT OF EXTERNAL PRESSURE AND CHEMICAL SUBSTITUTION ON THE PHASE TRANSITIONS IN MnAs

A. ZIĘBA
Institute of Physics and Nuclear Techniques, Academy of Mining and Metallurgy, 30–059 Cracow, Poland

R. ZACH
Institute of Physics, Technical University of Cracow, 30–084 Cracow, Poland

H. FJELLVÅG and A. KJEKSHUS
Department of Chemistry, University of Oslo, Blindern, N-0315 Oslo 3, Norway

(*Received* 10 *March* 1986; *accepted in revised form* 10 *July* 1986)

Abstract—The evolution of the phase transitions in $Mn_{1-t}T_tAs$ (T = Ti, V, Cr, Fe, Co and Ni) with t at low substitution levels is correlated with the external pressure, temperature (P, T) phase diagram of MnAs using the chemical pressure (P^*) concept. The study is based on data for transition temperatures and unit cell dimensions at atmospheric pressure and P, T phase diagrams of $Mn_{1-t}T_tAs$ with different T and t. Chemical pressure coefficients (ranging between $\epsilon = -52 \pm 2$ kbar for T = Ti and $\epsilon = 133 \pm 12$ kbar for T = Fe, assuming $P^* = \epsilon t$) are estimated from the location of the boundary of the essentially pressure driven NiAs, F to MnP, P or MnP, H_a type transition in the individual P, T phase diagrams. Different features of the chemical pressure concept are examined, such as the relation $P^* = \epsilon t$ and its break-down above a certain substitution level, the correlation between unit cell volumes and compressibility, and the non-hydrostatic character of P^* for these non-cubic phases.

1. INTRODUCTION

External pressure generally affects the characteristics of phase transitions. The consequences of externally produced pressures and pressure simulated effects accomplished by chemical substitution should at once be distinguished between. The latter phenomenon is variously referred to as the alloying effect, internal pressure, chemical pressure, etc. in the literature, chemical pressure being used throughout this paper.

The origin of the chemical pressure is the different spacial requirements of the solute and solvent atoms of a given solid solution phase. Hence, contrary to real pressure, the chemical pressure can be both positive and negative. The use of chemical pressure is in many respects more convenient than the application of hydrostatic or uniaxial pressure, allowing, e.g. experiments under atmospheric pressure or vacuum conditions. However, the influence is certainly not identical, and several additional features are attached to the latter.

The most fundamental change introduced by the formation of a solid solution is connected with the break-down of the translational invariance of the structure. This originates both from the distribution of different atoms over one sublattice (viz. concerns the very nature of solid solution) and the structural topology (viz. broadened distributions of the interatomic distances around the average values). The substitutional disorder affects in various ways all physical properties and may lead to entirely new phenomena, such as spin-glass behaviour of certain magnetic solid solution systems.

Complications are encountered when the solute and solvent atoms are non-randomly distributed over a given sublattice. Short range order (or chemical clustering) gives rise to smeared phase transitions and results which depend on the thermal history of the samples. Long range order (viz. complete or partial superstructure formation, usually at rather high substitution levels) leads to entirely new crystal structures. In fact, the degree of short and/or long range order is a worry for all solid solution studies.

Last, but not least, non-hydrostatic rather than hydrostatic conditions are accomplished by substitutional solid solution in non-cubic structures. More precisely, it is the directional dependence of the bonds which prevents complete resemblance or proportionality between chemical and external pressure.

The formulation of guide-lines for the chemical pressure (P^*) concept represents a difficult task. Generally chemical pressure manifests itself as any response of the crystal lattice to a given change in substitution. A reasonable requirement is that all qualitative features of the pressure, temperature (P, T) phase diagram for a given solid solvent (T) should be retained in the composition, temperature (t, T) phase diagram for its solid solution systems,

and that only the phase boundaries are shifted by the substitution. It is convenient to consider the P, T phase diagrams for different substitution levels (t) of a solid solution phase as made up of (roughly) additive contributions from a chemical component (which can be positive or negative) and an external (positive) pressure. This simple interpretation is useful for the evaluation of the P, T phase diagrams in sections 4 and 5. The shift of the P, T phase boundaries as a function of t can be used as a quantitative measure of the chemical pressure. Proportionality between chemical pressure and composition, viz. $P^* = \epsilon t$, is required as an operative criterion for this work.

MnAs is the only model substance which is considered in this paper whereas the generalization to other compounds is postponed to a forthcoming article.

2. ON MnAs AND $Mn_{1-t}T_tAs$

Manganese monoarsenide is in some respects a unique model substance for a careful examination of the chemical pressure concept. Six or more different phases of MnAs have been recorded [1–3] as a function of temperature and pressure, of which five are included in the extract of the P, T phase diagram shown in Fig. 1. The transition temperatures are (apart from the Néel temperature T_N) affected by the external pressure to an extent of many K per kbar. Substitution in the metal ($Mn_{1-t}T_tAs$; T = Ti–Ni) or non-metal ($MnAs_{1-x}X_x$; X = P, Sb) sublattice produces corresponding temperature shifts at the ~1% substitution level [8]. The serious disadvantage of MnAs is the non-cubic nature of both its modifications (hexagonal for the NiAs type and orthorhombic for the MnP type).

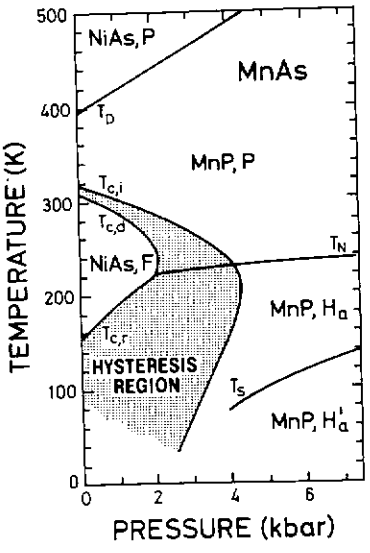

Fig. 1. P, T phase diagram for MnAs quoted from Ref. [1], taking account of additional evidences for structural and magnetic states in Refs [2–7]. Structural state is indicated by type designation, magnetic state by P (para), F (ferro) and H (helical). Transition temperatures are denoted by T_D for the MnP, P ⇄ NiAs, P type (distortion); T_N for Néel temperature; T_S for spiral change, and $T_{C,i}$, $T_{C,d}$ and $T_{C,r}$ for Curie temperatures on increasing, decreasing and re-entrant conditions, respectively. An MnP, F type state occurs above 7.5 kbar.

The object of the present study is to provide P, T phase diagrams for $Mn_{1-t}T_tAs$ with different T and t, and to use the obtained data as an experimental basis for testing of the chemical pressure concept. Prior to this work P, T phase diagrams for MnAs [1–3] and selected compositions of $Mn_{1-t}T_tAs$ with T = Ti [9, 10], Fe [11, 12] and Co [13] were at hand, but a more systematic charting of the various $3d$ metal substitutent systems was lacking. Fairly complete records of the structural and magnetic properties of all the $Mn_{1-t}T_tAs$ phases at atmospheric pressure are available [8, 14–24]. Unfortunately not very much experimental evidence is available on the effect of external pressure on the structural parameters of MnAs [2, 5].

A strategy of this investigation is to use the first order NiAs, F to MnP, P or MnP, H_a type transition (cf. Fig. 1) as a reference frame for other effects introduced by the chemical pressure in the $Mn_{1-t}T_tAs$ phases, and to estimate values for P^* from the location of the P, T phase boundary. This transition is essentially pressure driven, as implicated by the fact that the phase boundary is approximately perpendicular to the pressure axis of the P, T diagram, and furthermore it extends to 0 K. Since a phase transition at the absolute zero is driven by the difference in internal energy alone, we believe that the excess entropy introduced by turning to solid solutions will have a smaller impact on the NiAs, F to MnP, P or MnP, H_a type transition more than on the temperature driven MnP, P ⇄ NiAs, P type transition found at higher temperatures.

Values for P^* are estimated from the shifts in the extremal point P_E($P_{E,i}$ or $P_{E,d}$ depending on increasing or decreasing conditions) on the P vs T curve for $Mn_{1-t}T_tAs$ as compared with MnAs. As seen from Fig. 1, P_E defines the maximum pressure existence range of the NiAs, F type phase. In this way P^* is deduced from the measurements of the external pressure alone, no value of temperature being involved. P^* is thus represented as a scalar, which must be regarded as a crude, average approximation since P^* for a non-cubic substance should rather be characterized by a tensor.

Section 4 deals with the P, T phase diagrams for different t of the negative pressure phase $Mn_{1-t}Ti_tAs$. This system is especially suited for the experimental testing of the anticipated proportionality between P^* and t (see also section 1). The positive chemical pressure phases $Mn_{1-t}T_tAs$ with T = V, Cr, Fe, Co and Ni are treated in section 5. The changes in unit cell dimensions upon application of chemical pressure are discussed in section 6. Section 7 discusses the effect of chemical pressure on the transition temperatures T_D, T_C, T_N and T_S (cf. Fig. 1). The influence

of the chemical pressure is here conveniently summarized in dimensionless coefficients as $T_D^{-1}\partial T_D/\partial t$ and $T_C^{-1}\partial T_C/\partial t$. These can, in turn, be compared with $\epsilon T_D^{-1}\partial T_D/\partial P$ and $\epsilon T_C^{-1}\partial T_C/\partial P$ calculated from the chemical pressure coefficient (ϵ) for a given substituent (T) and the pressure derivatives ($\partial T_C/\partial P$, $\partial T_D/\partial P$) for MnAs.

3. EXPERIMENTAL

The polycrystalline samples of the $Mn_{1-t}T_tAs$ phases were prepared by repeated heat treatments of appropriate mixtures of MnAs and TAs (T = Ti–Ni). Details concerning the preparative procedure, and various structural and magnetic data for samples with corresponding compositions to those studied here are found in Refs [8, 15–24].

The homogeneity and structural state of the samples at atmospheric pressure were evaluated from X-ray powder diffraction photographs taken in a Guinier (room temperature) or Guinier Simon (below and above room temperature) camera. For more details concerning the X-ray diffraction work (including data reduction) see Ref. [7]. Section 6 is partly based on fresh structural data.

The pressure phase diagrams were determined from a.c. susceptibility (induction) measurements. The detection coils with the sample inside were placed in a Be–Cu pressure chamber, connected with a capillary tube to a 15 kbar helium gas compressor (UNIPRESS, Warsaw; model IF-012). A duplex sample pick-up coil arrangement was used to increase the measuring capacity.

Both temperature (P = const., i.e. isobaric condition) and pressure (T = const., i.e. isothermal condition) runs were used to locate the phase boundaries depending on their inclination. Figure 2 shows an isothermal run for $Mn_{0.97}V_{0.03}As$ as an example of the experimental procedure. The transition pressure for the NiAs, F to MnP, H_a (and vice versa) type transition is here (somewhat arbitrarily) chosen as the point where χ_{AC} equals half of its maximum value. (The same convention was adopted by Menyuk *et al.* [1].) Figure 2 demonstrates also the way of evaluating the degree of smearing of the transition (similarly for isobaric runs). The thus derived measures for the transition smearing are included as bars on the resulting P, T phase diagrams for $Mn_{0.97}V_{0.03}As$ and $Mn_{0.97}Co_{0.03}As$ in Fig. 3. (The inclination of the bar distinguishes between values recorded under isobaric and isothermal conditions.) The lengths of the bars in the two halves of Fig. 3 reflect the two extremes for the smearing situation observed in this study.

4. THE NEGATIVE PRESSURE PHASE $Mn_{1-t}Ti_tAs$

Crudely the chemical pressure reflects the difference in radius (size) between the solute and solvent atoms. Within the 3*d* element series the

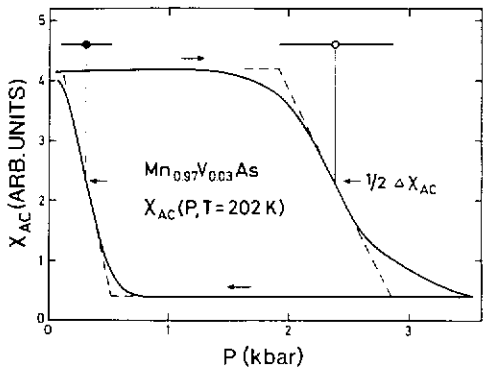

Fig. 2. Magnetic susceptibility χ_{AC} vs external pressure for an isothermal run for $Mn_{0.97}V_{0.03}As$. Transition pressure is chosen at $\frac{1}{2}\Delta\chi_{AC}$. Degree of smearing is represented by the bars, derived as shown on the illustration.

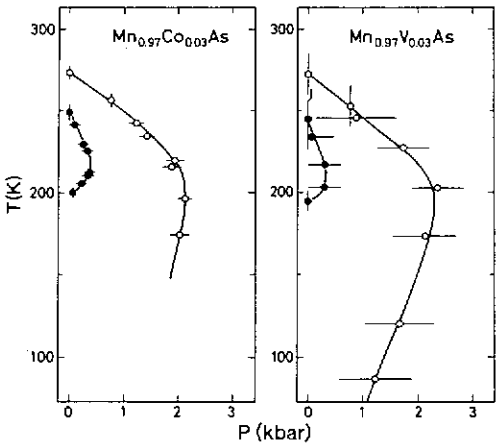

Fig. 3. P, T phase diagram data for $Mn_{0.97}V_{0.03}As$ and $Mn_{0.97}Co_{0.03}As$. Length of bars gives degree of smearing (see Fig. 2), horizontal and vertical bars refer to isothermal and isobaric runs, respectively.

(Pauling [25]) metallic radius decreases monotonically from Ti to Ni, and on this basis the substitution of Ti, V and Cr for Mn is expected to produce a negative pressure effect. The circumstance that this is not the case for V and Cr can be attributed to the fact that Mn, in $Mn_{1-t}T_tAs$ carries a large (partly localized) magnetic moment which increases the atomic size (cf. the discussion in Ref. [12]).

According to the structural data for the $Mn_{1-t}T_tAs$ phases (section 6), $Mn_{1-t}Ti_tAs$ represents the only negative chemical phase (viz. $V_{TiAs} > V_{MnAs}$). It is interesting to note that according to the prediction of the Bean Rodbell [26] model the first order NiAs, F to MnP, P type transition should convert to second order at some negative (chemical) pressure. Conversely, application of external pressure to a sample with a comparatively large negative chemical pressure should restore the first order character of the transition. These predictions have been confirmed for $Mn_{1-t}Ti_tAs$ by Val'kov *et al.* [9], who

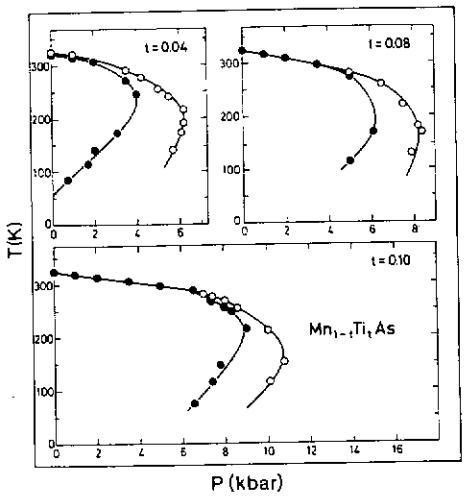

Fig. 4. P, T phase diagram data for $Mn_{1-t}Ti_tAs$ with $t = 0.04$, 0.08 and 0.10.

located the change of transition character at $t = 0.06$ for $P = 1$ bar. However, a more detailed examination of data for $Mn_{1-t}Ti_tAs$ [9, 22] reveals two discrepancies with the original Bean Rodbell [26] model. Firstly, $T_{C,i}$ and $T_{C,d}$ do not increase as rapidly as expected, but rather stay relatively constant for small t. Secondly, the change of the transition character occurs at a much lower t value than anticipated. However, both discrepancies can be explained semi-quantitatively when the effect of dilution of the Mn sublattice by non-magnetic Ti atoms is taken into account [22].

The evolution of the present P, T phase diagrams for $Mn_{1-t}Ti_tAs$ with increasing t is illustrated in Fig. 4 which appear to be consistent with those in Ref. [8]. In agreement with Val'kov *et al.* [8] the NiAs, F to MnP, P type transition is consistently of first order for samples with $0.00 \leqq t \leqq 0.06$. As indicated by the occurrence of hysteresis (see Fig. 4), the transition character shifts from second to first order upon increasing external pressure for $t = 0.08$ and 0.10. For $t = 0.08$ the first order character of the transition is observed at $P = 1$ kbar, but is lacking at atmospheric pressure. (With the scale used in Fig. 4 the opening of the hysteresis region first becomes visible at $P \approx 4.5$ kbar.) The change in transition order for $t = 0.10$ is tentatively assessed at $P \approx 3$ kbar, which is appreciably lower than $P = 5.1$ kbar reported in Ref. [9] for $t = 0.09$ [The corresponding diagram for, say, $t = 0.20$ is represented by a *single straight* (second order) T_C *line* up to $P = 14$ kbar with a slope of -3.75 K/kbar.] Hence, the tricritical point for $Mn_{1-t}Ti_tAs$ at atmospheric pressure, as estimated from the P, T phase diagrams, is located just below $t = 0.08$, viz. lies between the values $t \approx 0.06$ and $t \approx 0.10$ reported in Refs [9, 10] and [22], respectively.

The upper left corner of Fig. 5 shows the compositional variation of the extremal pressures $P_{E,d}$ and $P_{E,i}$, derived from the individual P, T phase diagrams as defined in section 2. Up to $t = 0.08$ $P_{E,d}$

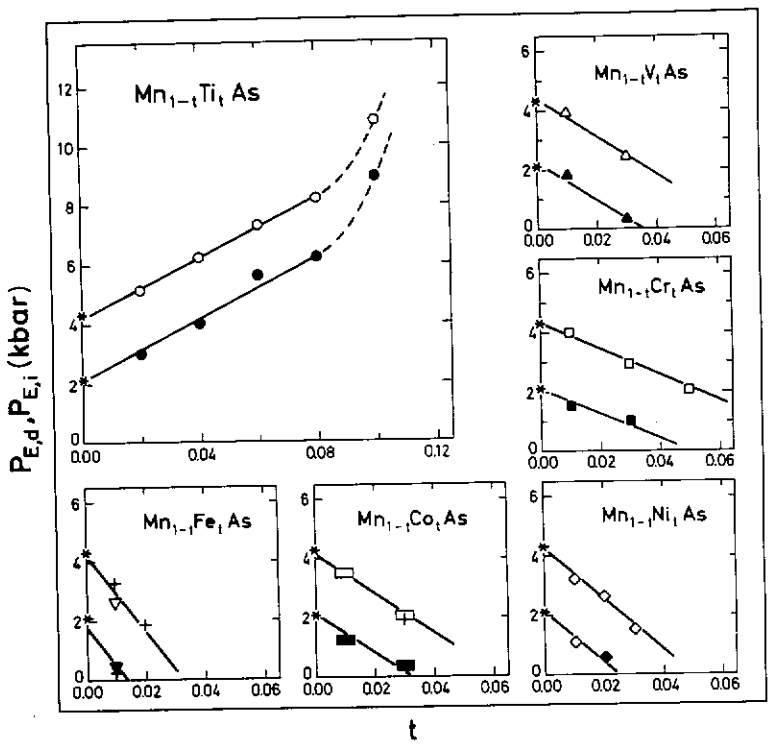

Fig. 5. External pressure $P_{E,d}$ and $P_{E,i}$ (see section 2 and caption to Fig. 1) vs t for $Mn_{1-t}T_tAs$ with T = Ti–Ni. Points marked (+) are quoted from Refs [11–13]. Lines represent least squares fits to experimental points, assuming that $P_{E,d}$ and $P_{E,i}$ define strictly parallel lines.

and $P_{E,i}$ are well represented by *parallel straight lines*, whereas for $t \geqq 0.10$ the extremal pressures increase markedly. Hence, according to the present operative criterion (see section 1) the chemical pressure concept is valid up to $t = 0.08$. The least squares fitted coefficient is $\partial P_E/\partial t = 52 \pm 2$ kbar (the error limits representing standard deviations calculated assuming that each experimental point for all systems studied carries the same mean standard error). The negative $\partial P_E/\partial t$ equals the chemical pressure coefficient ϵ, viz. $\epsilon = -52 \pm 2$ kbar for $Mn_{1-t}Ti_tAs$.

The non-equivalence of external and chemical pressures (see sections 1 and 2) can be demonstrated by the P, T phase diagram for, say, $t = 0.08$ in Fig. 4. For this composition the external and chemical pressures should be counterbalanced ($P + \epsilon t = 0$) at $P = 52 \times 0.08 = 4.2$ kbar. However, a shift of the ordinate axis to 4.2 kbar does clearly not provide a P, T phase diagram identical to that of MnAs (Fig. 1). The discrepancies, which concern important features of the diagram, should be ascribed to the non-cubic structure of the phases and to effects of dilution (see sections 6 and 7).

5. THE POSITIVE PRESSURE PHASES $Mn_{1-t}T_tAs$, T = V, Cr, Fe, Co and Ni

The P, T phase boundaries for $Mn_{1-t}T_tAs$ with T = V, Cr, Fe, Co and Ni are shifted towards lower pressures as compared with MnAs. This shows that the replacement of Mn with T = V–Ni in MnAs simulates the effect of a positive external pressure. Before considering the evolution of the P, T phase diagrams a few other observations should be briefly mentioned.

The transitions are smeared, probably as a result of an uneven distribution of Mn and T on the metal sublattice. The smearing is generally smaller for T = Fe and Co than for T = V and Cr (cf. Fig. 3 and section 3). This reflects inherent difficulties of a solid solution study and does not imply that the present samples are ill prepared.† The smearing found for, e.g. $Mn_{0.97}Co_{0.03}As$ (Fig. 3) is, in fact, about half of that recorded for MnAs itself by Menyuk *et al.* [1]. The degree of smearing increases with increasing pressure (i.e. is generally larger for the NiAs, F to MnP, P or MnP, H_a type transition than for the reverse transition at lower pressures).

The shifts of the P, T phase boundaries for $Mn_{0.99}T_{0.01}As$ with T = V–Ni (Fig. 6) depend in a rather unexpected way on the substituent T. The largest shifts of the phase boundaries are observed for Fe, then follow Ni, Co and V, and finally Cr. The same trend is also observed at the higher substitution levels, as is, e.g. seen for $Mn_{0.97}Co_{0.03}As$ and $Mn_{0.97}V_{0.03}As$ in Fig. 3.

The compositional variations in $P_{E,d}$ and $P_{E,i}$ (cf. section 2) for the $Mn_{1-t}T_tAs$ phases are shown in Fig. 3, which also includes *observations* quoted from Refs [11–13] for $Mn_{0.99}Fe_{0.01}As$, $Mn_{0.98}Fe_{0.02}As$ and $Mn_{0.97}Co_{0.03}As$. (Refs [11–13] also give extrapolated negative values for $P_{E,d}$ and/or $P_{E,i}$, but these are not considered here.) Similarly the present $Mn_{0.95}Cr_{0.05}As$ and $Mn_{0.97}Ni_{0.03}As$ samples only gave rise to $P_{E,i}$ values since these had to be converted into their *metastable* NiAs, F type state by the action of a magnetic field before the pressure experiments could be performed. The stability ranges (with respect to t of $Mn_{1-t}T_tAs$) for the positive chemical pressure phases of NiAs, F type cover much narrower composition ranges in Fig. 5 than their negative chemical pressure counterpart $Mn_{1-t}Ti_tAs$. Also for the positive pressure substituents, linear relationships prevail between $P_{E,d}$, $P_{E,i}$ and t (with constant difference $P_{E,i} - P_{E,d}$). The least squares fitted slopes, using all experimental points for each substituent (see also section 4), give (in kbar) $\epsilon = 64 \pm 7$ for T = V, $\epsilon = 44 \pm 5$ for T = Cr, $\epsilon = 133 \pm 12$ for T = Fe, $\epsilon = 67 \pm 6$ for T = Co and $\epsilon = 86 \pm 8$ for T = Ni. As judged from the unit cell volume (section 6) the ϵ value for T = Co is surprisingly low.

The variation of $P_{E,d}$ and $P_{E,i}$ with t may also be obtained from the magnetic field induced properties

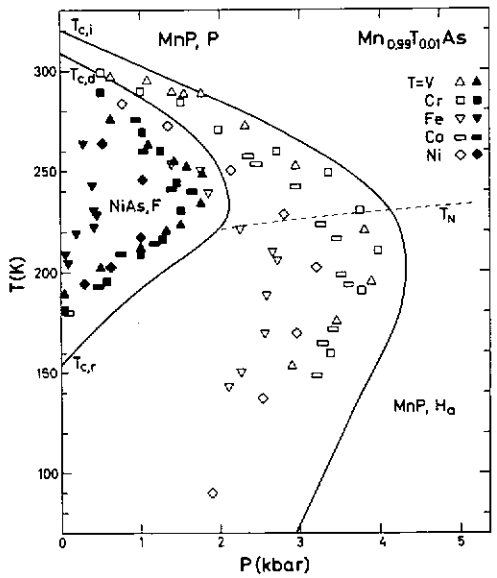

Fig. 6. P, T phase diagram data for $Mn_{0.99}T_{0.01}As$, T = V–Ni and MnAs (solid curves without data points, see also Fig. 1). Open and filled symbols refer to increasing and decreasing conditions, respectively. Legends to symbols are given on the illustration.

† A peculiar observation is that the samples appear to undergo some kind of "aging" phenomenon when they are stored for prolonged times at room temperature and atmospheric pressure. When such samples then were subjected to excess pressure for the *first time* at temperatures below ~200 K the NiAs, F to MnP, H_a type transition occurred at 10–50% higher pressures than in the succeeding runs. However, the phenomenon was not pursued further by us, and the results recorded for the "aged state" of the samples are not included in this report.

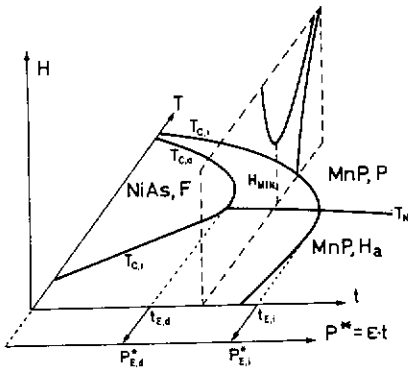

Fig. 7. Schematic H, $t(P^*)$, T phase diagram for $Mn_{1-t}T_tAs$ phases, with an intersecting plane in the latent ferromagnetic region. $t_{E,d}$ and $t_{E,i}$ refer to extremal points on the t, T phase boundaries; $P^*_{E,d}$ and $P^*_{E,i}$ to corresponding chemical pressures and H_{MIN} to the minimum critical field for release of latent ferromagnetism. Other notations are defined in the caption to Fig. 1.

of the $Mn_{1-t}T_tAs$ samples at atmospheric pressure. For the composition ranges in Fig. 5 with $P_{E,i} > 0$ and the extrapolated $P_{E,d} < 0$, latent ferromagnetism (viz. the NiAs, F type state) can be induced by the action of a strong magnetic field at atmospheric pressure. The relation between the compositional t, T and magnetic H, T phase diagrams for the latent ferromagnetic (LF) case is schematically illustrated in Fig. 7. The extremal values $t_{E,d}$ and $t_{E,i}$ in the t, T diagrams correspond to $P_{E,d}$ and $P_{E,i}$ (~ 2.1 and ~ 4.3 kbar, respectively) in the P, T phase diagram of MnAs. The composition range $0 < t < t_{E,d}$ is the domain of ferromagnetism at low temperature, $t > t_{E,i}$ that of helimagnetism, whereas for $t_{E,d} < t < t_{E,i}$ latent ferromagnetism can be induced (from an initial P or H_a state depending on the temperature) by a (strong) magnetic field.

Among the present samples, latent ferromagnetism is observed for $Mn_{0.95}V_{0.05}As$, $Mn_{0.95}Co_{0.05}As$ and $Mn_{0.97}Ni_{0.03}As$ (see also Refs [8, 23] whereas $Mn_{0.95}Cr_{0.05}As$ proved to be an F–LF border-line case). Val'kov *et al.* [12] report latent ferromagnetism for $Mn_{0.98}Fe_{0.02}As$. This information permits assessment of rough limits for ϵ using the inequalities $2.1/t_{LF} < \epsilon < 4.3/t_{LF}$. This gives $42 < \epsilon < 86$ kbar for $T = V$ and Co, and $\epsilon \approx 42$ kbar for the border-line case $T = Cr$. For $T = Ni$, $70 < \epsilon < 143$ kbar is obtained and since only a low critical field is required to trigger the transition the value is closer to the lower limit. The same procedure gives $105 < \epsilon < 215$ kbar for $T = Fe$. The reassuring conclusion is therefore that the different ways for estimation of ϵ give consistent values.

6. UNIT CELL DIMENSIONS AND THE CHEMICAL PRESSURE CONCEPT

The compositional variations of the unit cell dimensions at 10 (90) and 293 K for the $Mn_{1-t}T_tAs$ phases under consideration are compiled in Fig. 8. As indicated by the structural notations on the schematic t, T phase diagram in Fig. 7, two sets of unit cell dimensions should actually be considered at both temperatures. However, the NiAs, F type state exists only in very narrow composition intervals close to MnAs at 293 K for the positive chemical pressure phase, and the sparse structural data available for this temperature are not included here.

The external pressure effects described in sections 4 and 5 start from an initial NiAs, F type state. The pressure induced final states take the MnP, P or MnP, $H_a(H'_a)$ type structure (cf. Figs 1 and 7). Hence, the present chemical pressure considerations primarily address the NiAs, F type state, and the structural data for the MnP, P and MnP, H_a type states are used for supplementary purposes. As seen from Fig. 8(a) an increase in the unit cell volume takes place in the NiAs, F type state of $Mn_{1-t}Ti_tAs$ upon increasing t, just as expected for a negative chemical pressure phase. The opposite behaviour of the unit cell volumes for $Mn_{1-t}T_tAs$ with $T = V$, Cr, Fe, Co and Ni complies with their classification as positive chemical pressure phases. However, due to the very low substitution levels and the consequent minor changes in the unit cell dimensions observable for the positive chemical pressure phases, considerable uncertainties are associated with $\hat{\partial}V/\hat{\partial}t$ for these phases.

The trends in Fig. 8(a) fit the qualitative picture developed in section 5 in that $T = Fe$ and Ni constitute substituents with large, and $T = V$, Cr and Co substituents with moderate positive chemical pressure ability. Knowledge of the compressibility (K) of MnAs at 90 K should permit a comparison of the changes in the unit cell volume induced by external and chemical pressures. Grazhdankina and Burkhanov [27] and Dörfler and Bärner [28] report $K \approx 4.3 \times 10^{-3}$ kbar^{-1} at room temperature (derived by non-standard methods), and this value fits the results obtained by neutron diffraction by Sirota *et al.* [2]. According to the latter work $K = 1.5 \times 10^{-3}$ kbar^{-1} at 90 K (derived from only three experimental points). From the postulated relation $V_{Mn_{1-t}T_tAs}(T, t) = V_{MnAs} - V_{MnAs}\epsilon(T)tK_{MnAs}$ the induced volume change can be calculated, and the results are indicated by the dotted lines in Fig. 8(a). The overall agreement between calculated and observed volume changes is quite good (probably within estimated error limits when the uncertainties in V, ϵ and K are taken into account). The non-hydrostatic pressure effect simulated by substitution is, as evident from the variations in a and c with t [Fig. 8(a)], particularly striking for $T = Ti$ and V.

For the NiAs type structure there is a direct correlation between the unit cell volume and the metal to non-metal bond distance [29]. Hence, the trends brought out for V vs t in Fig. 8(a) also correspond to the variation in the Mn, T–As bond distance with t. The overall effect of 4% substitution of TiAs in MnAs is to increase the Mn, Ti–As

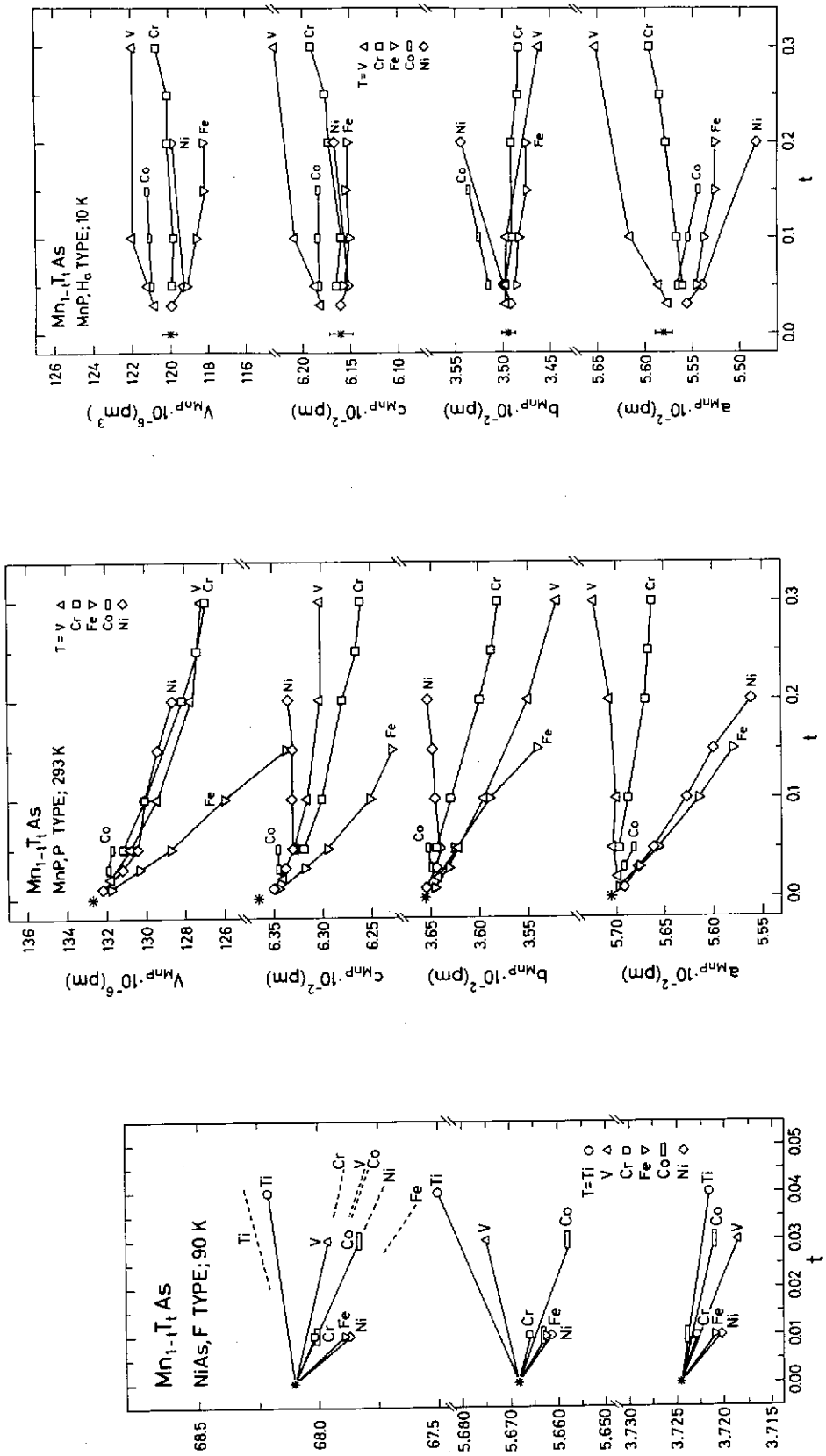

Fig. 8. Unit cell dimensions vs t for $Mn_{1-t}T_tAs$ with T = Ti–Ni. Data are mostly taken from Refs [15–24]. (a) NiAs, F type state at 90 K (this work). Broken lines refer to calculations described in the text; (b) MnP, P type state at 293 K, and (c) MnP, H_α type state at 10 K.

distance from 257.5 pm ($t = 0.00$) to 257.6 pm ($t = 0.04$); for $T = V$ and $t = 0.03$ the Mn, V–As distance has shrunk to 257.3 pm, while for $T = Fe$ (the substituent which shows the largest chemical pressure effect) the corresponding distance is 257.3 pm at $t = 0.01$. Thus rather small changes on the atomic scale are involved at these low substitution levels. A characteristic of the NiAs type structure is that the metal atoms are arranged in chains parallel to c, the shortest metal–metal separation being $c/2$. The increase in c with increasing substitution of VAs in MnAs probably reflects a weakening of the metal–metal interaction.

The overall picture of the variations of the crystal structure with substitution is strongly influenced by the fact that Mn can be in so-called high and low spin states or take any intermediate spin value [30, 31]. The terms high and low spin should not be interpreted too literally, although there are clear evidences for a marked distinction in the atomic size of Mn between the two electronic states. The NiAs, P and NiAs, F type phases correlate with high spin, the MnP, H_a type with low spin, while the whole range of intermediate spin values occurs for the MnP, P type state. The pressure induced transitions considered in sections 4 and 5 can almost certainly be labelled as high spin–low spin transitions associated with the discontinuous changes in structural parameters and magnetic order. There are no direct measurements of the spin state in the (external) pressure induced MnP, P and MnP, H_a type phases. However, such data are available for the positive chemical pressure, MnP, H_a type phases [6, 7, 14, 16–24, 32].

The variation in the unit cell dimensions for the MnP, P type state of the $Mn_{1-t}T_tAs$ phases at 293 K are shown in Fig. 8(b). Since these phases undergo a spin conversion (vide supra) around this temperature (correlated with rather large thermal expansion), it is reasonable to ascribe the irregularities in Fig. 8(b) to an additional size perturbation resulting from the variable spin state combined with the chemical pressure effect.

At temperatures below T_N (for the given combination T, t) the application of external pressure induces the NiAs, F to MnP, H_a type transition, most probably accompanied by a shift from high to low spin. The overall structural situation in the MnP, H_a type state (with low spin Mn) of the $Mn_{1-t}T_tAs$ phases is depicted in Fig. 8(c). According to the illustration $T = V$ and Co should here act as negative, Cr as neutral and Fe and Ni as positive chemical pressure substituents. These findings (except $T = Co$) are qualitatively consistent with the variation in the unit cell volume of low spin MnAs [4, 5] and the other binary TX phases [23], and hence also with the chemical pressure concept. (It is tempting to suggest that the electronic state of Co in MnP, H_a type $Mn_{1-t}Co_tAs$ ($0.05 < t \leqq 0.15$) differs from that in CoAs. Rather than turning to speculations, $Mn_{1-t}Co_tAs$ should be regarded as a candidate for re-examination.) The detailed description of the MnP type crystal structure requires knowledge of four unconstrained positional parameters in addition to three unit cell dimension. Such information is unfortunately lacking for the positive chemical pressure phases in the composition range close to MnAs (but is available for $t \geqq 0.05$). In the orthorhombic MnP type structure, both metal and non-metal atoms have a crystallographic freedom which allows various readjustments as easy relaxation to external and chemical pressures.

7. EFFECT OF CHEMICAL PRESSURE ON THE TRANSITION TEMPERATURES T_D, T_C, T_N AND T_S

A natural challenge for the chemical pressure concept in relation to the $Mn_{1-t}T_tAs$ phases is that it should be able to relate the effects of substitution and external pressure on the different transition temperatures T_D, T_C, T_N and T_S (cf. Fig. 1). The distortion temperature T_D refers to the continuous, displacive MnP, P $\rightleftarrows$ NiAs, P type transition (soft mode character) in $Mn_{1-t}T_tAs$ [7, 15, 33, 34]. The NiAs, F to MnP, P type transition at T_C [4] implies disordering of the magnetic moments, but a strong magnetoelastic coupling and differences in the atomic arrangement above and below T_C make it first order with an appreciable hysteresis. The MnP, $H_a \rightleftarrows$ MnP, P type transition at T_N, which involves ordering–disordering of the magnetic moments, is usually of second order, but is discontinuous with appreciable jump in unit cell volume for $Mn_{1-t}Cr_tAs$ [35–37] and $Mn_{1-t}Ni_tAs$ [23]. The slight rearrangement of the helical spin structure at T_S is discussed only briefly due to partly lacking or uncertain determination of this phase boundary.

The transitions at T_D, T_C, T_N and T_S concern quite different physical phenomena, and it is not at all obvious or trivial that they should show a homogeneous relation to the chemical pressure. However, it is an encouraging fact that both crystallographic and magnetic structures are directly correlated with the various bonding interactions. The main emphasis is put on T_C and T_D since these transitions take place at low substitution levels (including $t = 0$), where the operational chemical pressure criterion $P^* = \epsilon t$ should hold. The magnetic transitions at T_N and T_S which are found at higher substitution levels are discussed more briefly. The change in a given transition temperature T_Y (Y = D, C, N or S) as a function of substitution is systematized in terms of the dimensionless coefficient $T_Y^{-1}\partial T_Y/\partial t$.

Starting with T_C, the concentration derivatives of the Curie temperature were determined from $T_{C,i}(t)$ for the ferromagnetic region ($0 < t < t_{E,d}$). The reason for this choice is that the corresponding phase boundary $T_{C,i}(P)$ for MnAs [1] varies approximately linearly for $0 < P < P_{E,d}$. The experimental values for the normalized derivatives $T_C^{-1}\partial T_C/\partial t_C$ (calculated

from the data in Refs [8, 22, 23], assuming the same error for all $T_{C,i}$ in the accuracy assessments) are shown in Fig. 9, and compared with those derived from $\epsilon T_C^{-1} \partial T_C/\partial P_C$ using ϵ from sections 2, 4 and 5; and $\partial T_C/\partial P = -17$ K/kbar for MnAs [1]. The illustration brings out a reasonably good agreement between the experimental ($T_C^{-1}\partial T_C/\partial t$) and predicted ($\epsilon T_C^{-1} \partial T_C/\partial P$) action of the chemical pressure. The observation that $T_C^{-1}\partial T_C/\partial t$ tends to take lower values than $\epsilon T_C^{-1}\partial T_C/\partial P$ for T = Ti, V, Co and Ni may be explained as an effect of dilution on the Mn sublattice by the essentially non-magnetic substituents. (Dilution in $Mn_{1-t}Ti_tAs$ is discussed in Ref. [22]. The substituents T = Cr and Fe very probably carry a magnetic moment in their $Mn_{1-t}T_tAs$ phases.) Different theories [38] predict that $T_C^{-1}\partial T_C/\partial t$ should be *lowered* by about 1 (or more) upon dilution and the difference ($\epsilon T_C^{-1}\partial T_C/\partial P - T_C^{-1}\partial T_C/\partial t$) is roughly consistent with this prediction for T = Ti, V, Co and Ni. (Note that MnAs has an unusually large pressure derivative for T_C. Consequently, it is quite natural to assume that the effect of chemical pressure on T_C in these phases is important, whereas the effect of dilution plays a much larger role in most systems. On the other hand, if the effects of dilution are in focus one should choose systems with a negligible chemical pressure [38].)

The experimental values for the normalized derivatives $T_D^{-1}\partial T_D/\partial t$ are extracted from all available data for $Mn_{1-t}T_tAs$ [14–24, 35, 36] (generally $0 \leqq t \leqq 0.10$, but using the full linear T_D vs t range in the error assessments when such relationships exist.) For the calculation of $\epsilon T_D^{-1}\partial T_D/\partial P$, $\partial T_D/\partial P = 23$ K/kbar for MnAs [1] is used. The comparison between (experimental) $T_D^{-1}\partial T_D/\partial t$ and (predicted) $\epsilon T_D^{-1}\partial T_D/\partial P$ (Fig. 9) shows that the predictions for the effect of the chemical pressure on T_D are quite good for T = Ti, V and Cr, but rather poor for T = Fe, Co and Ni. It may be significant to note that this grouping separates the substituents with lighter atomic masses (or lower atomic numbers) from those with heavier. Even for the substituents Fe, Co and Ni there is a definite correlation between $T_D^{-1}\partial T_D/\partial t$ and $\epsilon T_D^{-1}\partial T_D/\partial P$ suggesting that the chemical pressure still has a major influence on the compositional dependence of T_D. Atomic mass is definitely a factor (irrelevant for magnetic transition) which enters in soft mode type transitions, but it is difficult to explain why this should not be equally important for both lighter and heavier substituents.

The MnP, $H_a \rightleftarrows$ MnP, P transition temperature T_N increases only slightly with increasing pressure, $\partial T_N/\partial P = 1.4$ K/kbar for $P > 5$ kbar according to Ref. [1]. This value together with the ϵ values for the different substituents allows calculation of the derivative $\epsilon T_N^{-1}\partial T_N/\partial P$. These data are compared in Fig. 9 with the observed derivative $T_N^{-1}\partial T_N/\partial t$, estimated from Refs [8, 16–18, 21, 23]. $T_N^{-1}\partial T_N/\partial t$ is seen to take small negative values, whereas $\epsilon T_N^{-1}\partial T_N/\partial P$ is numerically similar, but of opposite sign. The distinction between corresponding values is also here mainly due to dilution since the difference ($\epsilon T_N^{-1}\partial T_N/\partial P - T_N^{-1}\partial T_N/\partial t$) is roughly 1. In $MnAs_{1-x}P_x$, where the magnetic sublattice remains undiluted throughout the entire solid solution range, T_N increases with increasing x and behaves accordingly as expected for a positive chemical pressure phase. Using a reasonable estimate $53 < \epsilon < 107$ kbar (obtained from the occurrence of latent ferromagnetism in $MnAs_{0.96}P_{0.04}$ [39]) one arrives at $0.4 < \epsilon T_N^{-1}\partial T_N/\partial P < 0.7$ which compares rather well with the observed value of $T_N^{-1}\partial T_N/\partial x = 0.9$ for $MnAs_{1-x}P_x$ [6].

The MnP, $H_a' \rightleftarrows$ MnP, H_a transition (at T_S) can be discussed only for $MnAs_{1-x}P_x$ since relevant data are lacking for $Mn_{1-t}T_tAs$. For $MnAs_{1-x}P_x$ qualitative consistency can be recorded as T_S is found to increase both with increasing pressure (P) and substitution (x). There is also consistency between the position of the H_a', H_a, F triple point at $P = 7.5$ kbar in the P, T phase diagram of MnAs [1] and the corresponding point at $x = 0.09$ in the x, T phase diagram of $MnAs_{1-x}P_x$ [6, 7].

The generally more favourable application of the chemical pressure idea to $MnAs_{1-x}P_x$ than to $Mn_{1-t}T_tAs$ appears to result from the unchanged magnetic sublattice and the constant number of valence electrons in the former phase.

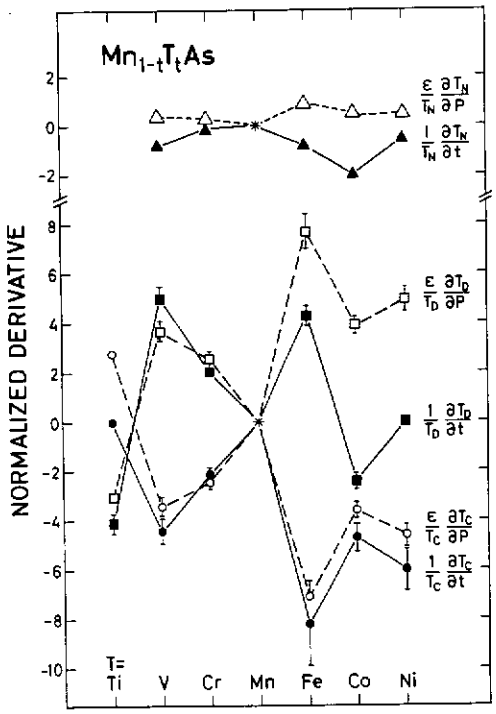

Fig. 9. Comparison of observed (filled symbols) and calculated (open symbols) normalized temperature derivatives for the NiAs, F to MnP, P (T_C), MnP, P $\rightleftarrows$ NiAs, P (T_D) and MnP, P $\rightleftarrows$ MnP, H_a (T_N) type transitions for $Mn_{1-t}T_tAs$ with T = Ti–Ni. For the calculated values see text.

8. CONCLUSIONS

The large amount of experimental data for the $Mn_{1-t}T_tAs$ and $MnAs_{1-x}X_x$ solid solution phases have been rationalized according to the chemical pressure concept. The outcome contributes to an improved understanding of the properties of MnAs and its solid solution derivatives and serves also to test different anticipated features of chemical pressure. A wider range of phases will be covered in the forthcoming paper.

The evaluation of the phase transitions in $Mn_{1-t}T_tAs$ and $MnAs_{1-x}X_x$ with t and x, respectively, at low substitution levels correlates generally favourably with the P, T phase diagram of MnAs. The variations in the magnetic order–disorder transition temperatures T_C and T_N for the $Mn_{1-t}T_tAs$ phases can be accounted for as the additive action of chemical pressure and dilution on the Mn, T sublattice. The corresponding variations of the structural transition temperature T_D may also be explained by the chemical pressure for T = Ti, V and Cr, whereas the reason for the poorer fit between experimental and calculated data for T = Fe, Co and Ni is not understood. The semiquantitative accordance between P, T and t, T phase diagrams in terms of the phase boundaries at T_D, T_C and T_N covers a number of $Mn_{1-t}T_tAs$ solid solution phases. A brief analysis of $MnAs_{1-x}P_x$ suggests full conformity between P, T and x, T phase diagrams. The latter finding reflects the fact that the magnetic sublattice remains intact and the number of valence electrons is constant in $MnAs_{1-x}P_x$.

The analyses have also picked out phases which deviate from the overall pattern of chemical pressure. The chemical pressure coefficient ϵ for $Mn_{1-t}Co_tAs$ is much smaller than expected from the unit cell volumes of MnAs and CoAs, the decrease in T_D with increasing Co content is anomalous, and T_N decreases more rapidly with t than for the other $Mn_{1-t}T_tAs$ phases. The marked minimum in T_C at $x \approx 0.2$ for the negative chemical pressure phase $MnAs_{1-x}Sb_x$ [40] can also hardly be explained in terms of chemical pressure and dilution. These phases are clear candidates for re-examination, and this work has in fact already been started.

The linear relation $P^* = \epsilon t$ *and its limits*

These are important features of the chemical pressure concept itself. Firstly, the most convenient and direct way to measure the chemical pressure is to utilize the shift with composition in a pressure driven transition in the P, T phase diagram. The experimental data for $Mn_{1-t}Ti_tAs$ reveal proportionality between P^* and t up to $t \approx 0.08$. The existence of such a limit is quite plausible since the inherent character of the host lattice (i.e. peculiarities of the bonds) necessarily must be affected at a certain substitution level. We are not aware of an experimental test of this aspect for other solid solution systems. The chemical pressure corresponding to $t = 0.08$ in $Mn_{1-t}Ti_tAs$ amounts to $P^* = -4.2$ kbar, which gives an indication of the order of magnitude of the chemical pressures generated in solid solution phases.

The relation to compressibility and unit cell dimensions

This is another aspect open for testing in terms of chemical pressure. The relation $\Delta V/V = PK$ represents merely the definition of the compressibility (K). However, when P is replaced by P^* the relation is not at all obvious, but the simple equation may be used to provide a test of the self-consistence of the chemical pressure concept. A comparison of the observed unit cell volumes for the NiAs, F type state at low temperature with calculated data according to the above relation and a rather approximate value for the compressibility of MnAs, reveals a rough, but promising degree of accordance. Some of the mismatches between the observed and calculated values for ΔV may originate from the inaccuracies in V and K, but the non-hydrostatic nature of P^* in different structural states of $Mn_{1-t}T_tAs$ probably also plays a considerable role. There is an overall consistence between chemical pressures and unit cell volumes.

The non-hydrostatic character of the chemical pressure in non-cubic phases

This is clearly demonstrated by the unit cell dimensions of the $Mn_{1-t}T_tAs$ phases. However, this aspect cannot be fully appreciated before the external pressure dependences of the unit cell dimensions of MnAs become available. The non-hydrostatic character of P^* is perhaps the most important obstacle to the general use of the chemical pressure concept.

Acknowledgements—The authors are grateful to the Norwegian Research Council for Science and the Humanities for financial support. A.Z. would like to express his appreciation for the hospitality he was shown at the University of Oslo, where this work was completed.

REFERENCES

1. Menyuk N., Kafalas J. A., Dwight K. and Goodenough J. B., *Phys. Rev.* **177,** 942 (1969).
2. Sirota N. N., Vasilev E. A. and Govor G. A., *J. Phys. (Paris)* **32-C1,** 987 (1971).
3. Gribanov I. F., Zavadskii E. A. and Sivachenko A. P., *Fiz Nizk. Temp.* **5,** 1219 (1979); *Soviet J. low-temp. Phys.* **5,** 577 (1979).
4. Zięba A., Selte K., Kjekshus A. and Andresen A. F., *Acta Chem. Scand.* **A32,** 173 (1978).
5. Andresen A. F., Fjellvåg H. and Lebech B., *J. Magn. Magn. Mater.* **43,** 158 (1984).
6. Fjellvåg H., Andresen A. F. and Bärner K., *J. Magn. Magn. Mater.* **46,** 29 (1984).
7. Fjellvåg H., Kjekshus A. and Stølen S., *J. Solid St. Chem.* **64,** 123 (1986).
8. Selte K., Kjekshus A., Andresen A. F. and Zięba A., *J. Phys. Chem. Solids* **38,** 719 (1977).

9. Val'kov V. I., Zavadskii E. A. and Todris B. M., *Fizika tverd. Tela* **19,** 235 (1977); *Soviet Phys. Solid St.* **19,** 134 (1977).
10. Ido H., Suzuki T. and Iguchi I., *J. Magn. Magn. Mater.* **31–34,** 159 (1983).
11. Galkin A. A., Zavadskii E. A., Smirnov V. M. and Val'kov V. I., *ZhETF Pis. Red.* **20,** 253 (1974); *JETP Lett.* **20,** 111 (1974).
12. Val'kov V. I., Zavadskii E. A. and Smirnov V. M., *Fizika tverd. Tela* **18,** 267 (1976); *Soviet Phys. Solid St.* **18,** 156 (1976).
13. Galkin A. A., Zavadskii E. A., Smirnov V. M. and Val'kov V. I., *Dokl. Akad. Nauk SSSR* **218,** 552 (1974); *Soviet Phys. Dokl.* **19,** 593 (1975).
14. Kazama N. and Watanabe H., *J. phys. Soc. Japan* **30,** 1319 (1971).
15. Selte K., Kjekshus A. and Andresen A. F., *Acta Chem. Scand.* **27,** 3607 (1973).
16. Selte K., Kjekshus A. and Andresen A. F., *Acta Chem. Scand.* **A28,** 61 (1974).
17. Selte K., Kjekshus A., Valde G. and Andresen A. F., *Acta Chem. Scand.* **A30,** 8 (1976).
18. Selte K., Kjekshus A., Valde G. and Andresen A. F., *Acta Chem. Scand.* **A30,** 468 (1976).
19. Selte K., Kjekshus A., Peterzéns P. G. and Andresen A. F., *Acta Chem. Scand.* **A30,** 671 (1976).
20. Delphin I. L. A., Selte K., Kjekshus A. and Andresen A. F., *Acta Chem. Scand.* **A32,** 179 (1978).
21. Selte K., Kjekshus A., Peterzéns P. G. and Andresen A. F., *Acta Chem. Scand.* **A32,** 653 (1978).
22. Zięba A., Fjellvåg H. and Kjekshus A., *J. Phys. Chem. Solids* **46,** 275 (1985).
23. Fjellvåg H., Kjekshus A., Andresen A. F. and Zięba A., *J. Magn. Magn. Mater.* **61,** 61 (1986).
24. Fjellvåg H., Kjekshus A. and Andresen A. F., *Acta Chem. Scand.* (To be published).
25. Pauling L., *The Nature of the Chemical Bond,* Cornell University Press, Ithaca, New York (1960).
26. Bean C. P. and Rodbell D. S., *Phys. Rev.* **126,** 104 (1962).
27. Grazhdankina N. P. and Burkhanov A. M., *Zh. Teor. Eksper. Teor. Fiz.* **50,** 1519 (1966); *Soviet Phys. JETP* **23,** 1013 (1966).
28. Dörfler M. and Bärner K., *Phys. Status Solidi* (*a*) **17,** 141 (1973).
29. Fjellvåg H. and Kjekshus A., *Acta Chem. Scand.* **A40,** 8 (1986).
30. Haneda S., Kazama N., Yamaguchi Y. and Watanabe H., *J. phys. Soc. Japan* **42,** 31 (1977).
31. Krokoszinski H. J., Santandrea C., Gmelin E. and Bärner K., *Phys. Status Solidi* (*b*) **113,** 185 (1982).
32. Haneda S., Kazama N., Yamaguchi Y. and Watanabe H., *J. phys. Soc. Japan* **42,** 1212 (1977).
33. Selte K. and Kjekshus A., *Acta Chem. Scand.* **27,** 3195 (1973).
34. Franzen H. F., Haas C. and Jellinek F., *Phys. Rev.* **B10,** 1248 (1974).
35. Fjellvåg H. and Kjekshus A., *Acta Chem. Scand.* **A38,** 1 (1984).
36. Fjellvåg H. and Kjekshus A., *Acta Chem. Scand.* **A39,** 671 (1985).
37. Zięba, A., Fjellvåg H. and Kjekshus A., *J. Magn. Magn. Mater.* (To be published).
38. De Jongh L. J., In *Magnetic Phase Transitions* (Edited by M. Auslos and R. J. Elliott). Springer, Berlin (1983).
39. Zięba A., Haneda S., Yamaguchi Y. and Watanabe H., *Phys. Status Solidi* (*a*) **5,** K27 (1979).
40. Edwards L. R. and Bartel L. C., *Phys. Rev.* **B5,** 1064 (1972).